Solution-processable and Photo-programmable Logic Gate Realized by Organic Non-volatile Floating-gate Photomemory

Yu-Dao Lu,[a,#] *Chan-Rung Hsu,* [a,#] *Shin-Hau Ke*,[a] *Kuan-Lin Lai*,[a] *Horng-Long Cheng,*[a,b,c] *Yu-Wu Wang*,[d] *Jung-Yao Chen,*[a,b,c*]

Table S1. The absorbance of N_3 stretching and the corresponding nitrene-forming efficiency evaluated from FTIR.

Exposure time (min)	N2200 and azide blend film		DPP-DTT and azide blend film		BCP and azide blend film	
	Absorbance of N_3 stretching	Efficiency[a] (%)	Absorbance of N_3 stretching	Efficiency[a] (%)	Absorbance of N_3 stretching	Efficiency[a] (%)
Baseline	0.00756	N/A	0.37472	N/A	0.00119	N/A
0	0.01282	0.00	0.37957	0.00	0.15704	0.00
10	0.01180	19.39	0.37853	21.44	N/A	N/A
20	0.01034	47.15	0.37580	77.73	N/A	N/A
30	0.01006	52.47	0.37536	86.80	0.07948	49.77

[a] Given that the formation of nitrene is the photolysis of N_3, the nitrene-forming efficiency can be traced by the variation of absorbance of N_3 in FTIR under UV light exposure. Based on the absorbance of N_3 stretching signal in the FTIR spectra of N2200 and azide blend film, DPP-DTT and azide blend film and BCP and azide blend film, the nitrene-forming efficiency can be calculated using the following formula:

$$\text{Efficiency}=\left\{1-\frac{(A_X-A_{baseline})}{(A_0-A_{baseline})}\right\}\times 100\% \tag{S1}$$

Where A_X is the absorbance of N_3 stretching at exposure time of x min, A_0 is the initial absorbance of N_3 stretching and A_{baseline} stands for the absorbance of baseline.

Table S2. AFM images and height profiles of photopatterned BCP films with different BCP to azide weight ratios. [a] Film retention was calculated by thickness of developed film/thickness of as-spun film*100%.

BCP:azide weight ratio	As-spun film		Developed film		Film retention [a]
	Height image	1D profile	Height image	1D profile	
1:1	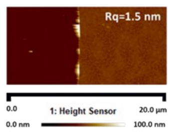	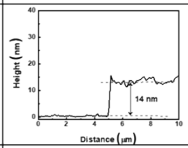	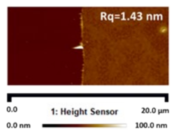	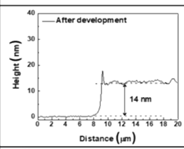	100%
1:2	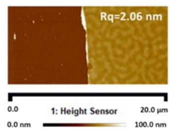	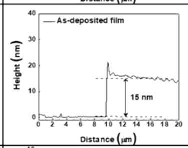	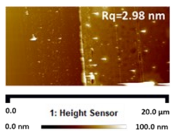	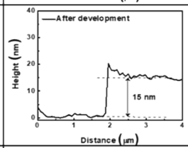	100%
1:4	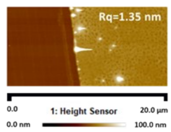	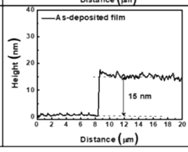	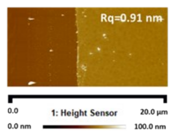	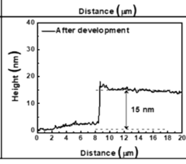	100%

Table S3. TRPL fitting results of BCP/ZnTPP and BCP/ZnTPP/N2200 under the excitation wavelength of 372 nm.

Sample	A_1	τ_1 (ns)	A_2	τ_2 (ns)	$\tau_{average}$ (ns)	CTE (%)
$S_1 \rightarrow S_0$						
BCP/ZnTPP	288.79	0.49	35.93	2.68	0.74	77
BCP/ZnTPP/N2200	90474.1	0.17	144.6	0.91	0.17	
$S_2 \rightarrow S_0$						
BCP/ZnTPP	74. 44	0.01	8903.5	0.45	0.45	67
BCP/ZnTPP/N2200	1.19	0.15	147	0.80	0.15	

Table S4 The organic photomemories with *n*-type charge-transporting materials and the corresponding electrical performance.

Charge-trapping material/ Charge-transporting material	**Light wavelength (nm)**	**Lowest Photo-programming time (s)**	**Light intensity (mW cm^{-2})**	**On/Off current ratio**	**Memory window (V)**	**Photoresponsivity (AW^{-1})**	**The deposited method for charge-transporting material**	**Reference**
PVSK / BPE-PTCDI	530	60	10	10^3	14	0.002	Thermal evaporation	*ACS Appl. Mater. Interfaces* 2021, 13, 20417−20426
SoI-PDI/ BPE-PDI	405	20	10	10^5	7.8	0.2	Thermal evaporation	*Adv. Mater.* 2020, 32, 2002638
C_{70} /C_{60}	white LED	50 ms & V_g = 22 V	3.76	N/A	2.5	N/A	Thermal evaporation	*Sci. Rep.* 2016, 6, 30536
PVA/C_{60}	405 nm	60	0.13	N/A	69.3	N/A	Thermal evaporation	*Phys. Chem. Chem. Phys.*, 2016, 18, 13108--13117
PVAn/QD/ PEPTC	450	10	14	10^4	14	0.0143	Thermal evaporation	*ACS Appl. Mater. Interfaces* 2023, 15, 1, 1675–1684
PDVT-10/ N2200	white	1	5	10^5	10	5	Spin coating	*ACS Photonics* 2021, 8, 10, 3094–3103
PPylr/C8-NDI	455	30	N/A	10^3	15	N/A	Thermal evaporation	*ACS Photonics* 2023, 10, 12, 4509–4518
TIPS-4/C8-PDI	530	10	5	10^4	N/A	0.004	Thermal evaporation	*Adv. Funct. Mater.* 2024, 2416306
ZnTPP/ N2200	405	0.1	59.73	10^5	18	0.00125	Spin coating	This work

Table S5. The state-of-the-art organic transistor-based neuromorphic devices.

Semiconductor	Device type	Classification tasks	Accuracy	Reference
Pentacene	Organic field-effect transistor	Handwritten digits	63.21%	*Small* **2021**, *17*, 2103837.
(Poly[2,5-bis(2-octyldodecyl)pyrrolo[3,4-c]pyrrole-1,4(2H,5H)-dione-3,6-diyl)-alt-(2,2′;5′,2″;5″,2‴-quaterthiophen-5,5‴-diyl)](PDPP4T)/chhlorophyll-a	Organic field-effect transistor	Handwritten digits	79%	*Npj Flex. Electron.* **2022**, *6*, 30.
2-hexylthieno[4,5-b][1] benzothieno[3,2-b][1] benzothiophene (BTBTT6-syn)	Organic field-effect transistor	Handwritten digits	90%	*Nat. Commun.* **2023**, *14*, 2281.
Poly(3-hexylthiophene-2,5-diyl)(P3HT)/[6,6]-phenyl-C61-butyric acid methyl ester(PCBM)	Organic ion-gated transistor	Fashion products	89.5%	*Nat. Photonics* **2023**, *17*, 629.
Poly[2,5-(2-octyldodecyl)-3,6-diketopyrrolopyrrole-alt-5,5-(2,5-di(thien-2-yl)thieno [3,2-b]thiophene)](DPPDTT) /Matrimid 5218(MI)	Organic field-effect transistor	Handwritten digits	50~80%	*Adv. Mater.* **2023**, 2310155.
2-(4,5-bis(4-fluorophenyl)-1-phenyl-1H-imidazol-2-yl)-4-(di(naphthalen-2-yl)amino)phenol(DNH-F)	Memristor	RGB color images	90%	*Nat. Commun.* **2023**, *14*, 5775.
Pentacene	Organic field-effect transistor	Handwritten digits	94.8%	*ACS Nano* **2023**, 17, 24, 25552.
DPPDTT	Organic ion-gated transistor	Handwritten digits	97.21%	*Adv. Mater.* **2024**, 36, 2312473.
2,7-dioctyl[1]benzothieno[3,2-b][1]benzothiphen (C8-BTBT)	Organic field-effect transistor	Handwritten digits	93.9%	*Chem. Eng. J.* **2024**, 498, 155237
N2200/ZnTPP	Organic non-volatile photomemory	Handwritten digits	94.66%	This work

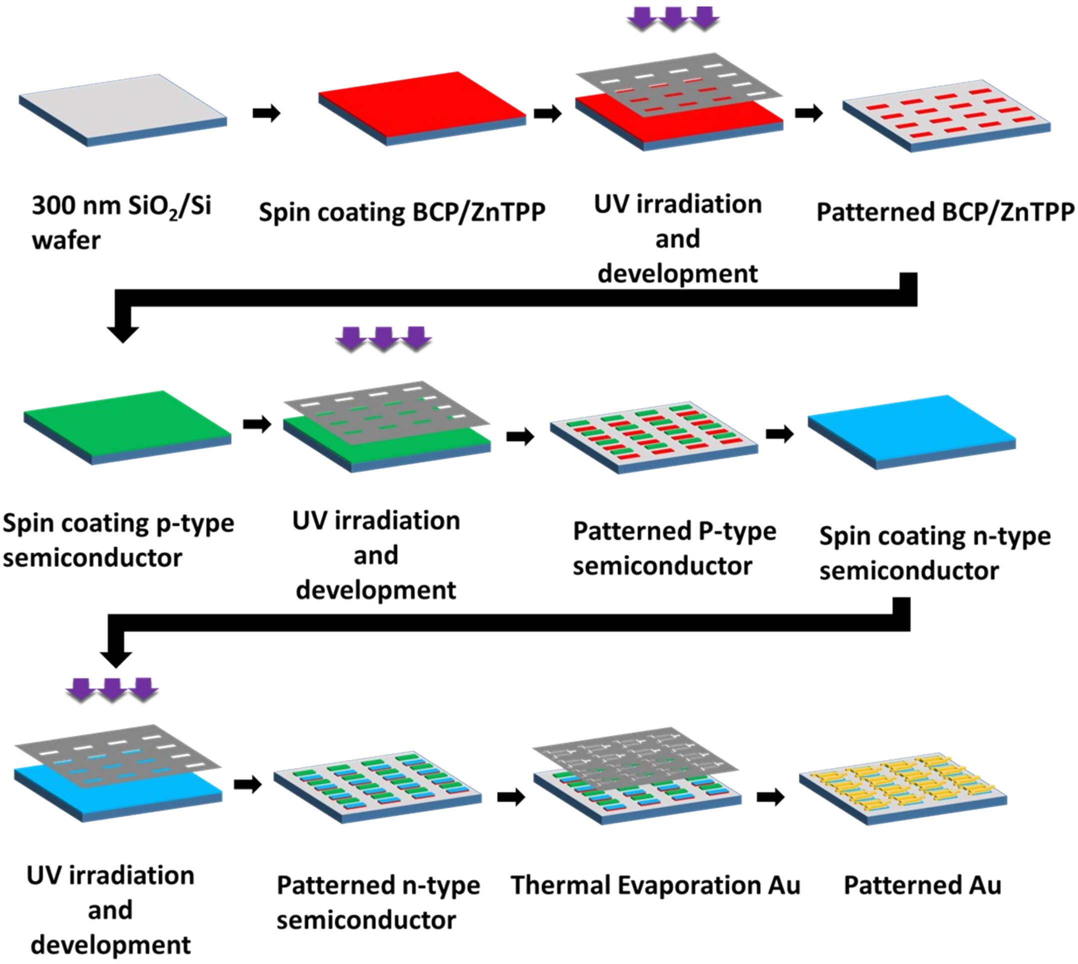

Figure S1. Schematic description of the fabrication processes for photopatterned and photo-programmable logic gate through photopatterning using azide as photo-crosslinker.

(a)

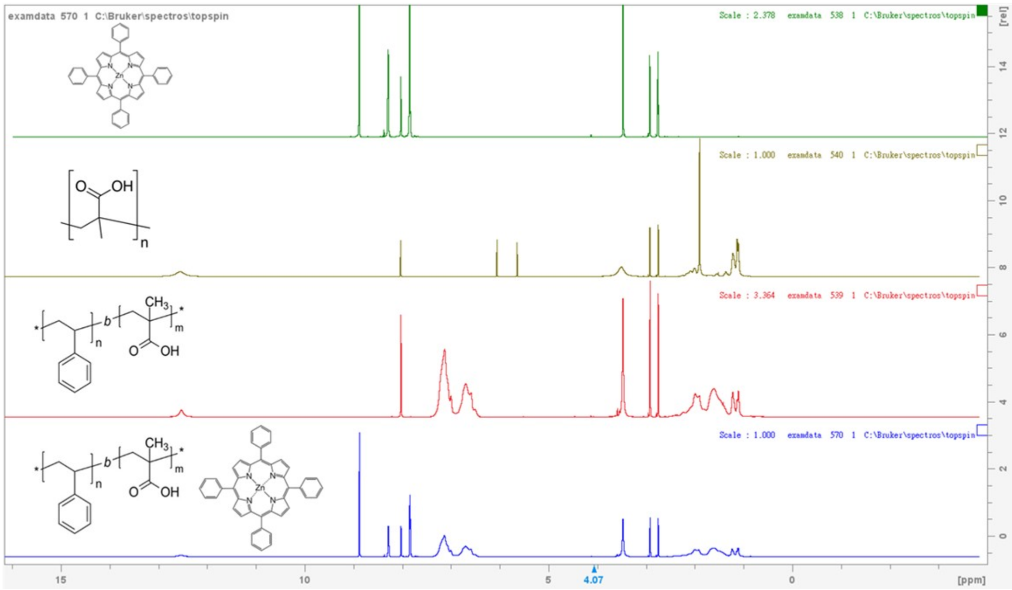

examdata 570 1 C:\Bruker\spectros\topspin
OH
CH3
OH
CH3
OH
[ppm]
15
10
5
4.07
0

(b)

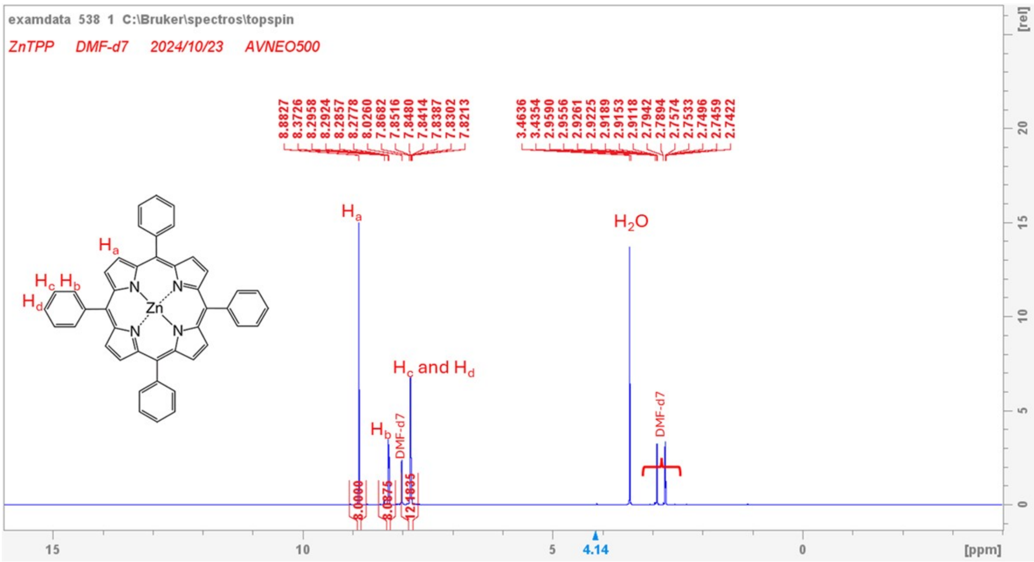

examdata 538 1 C:\Bruker\spectros\topspin
ZnTPP DMF-d7 2024/10/23 AVNEO500
8.8827 8.3726 8.2958 8.2924 8.2857 8.2778 8.0260 7.8682 7.8516 7.8480 7.8414 7.8387 7.8302 7.8213
3.4636 3.4354 2.9590 2.9556 2.9261 2.9225 2.9189 2.9153 2.9118 2.7942 2.7894 2.7574 2.7533 2.7496 2.7459 2.7422
Ha
H2O
Hc and Hd
Hb
DMF-d7
DMF-d7
Zn
[rel]
[ppm]
15
10
5
4.14
0

(c)

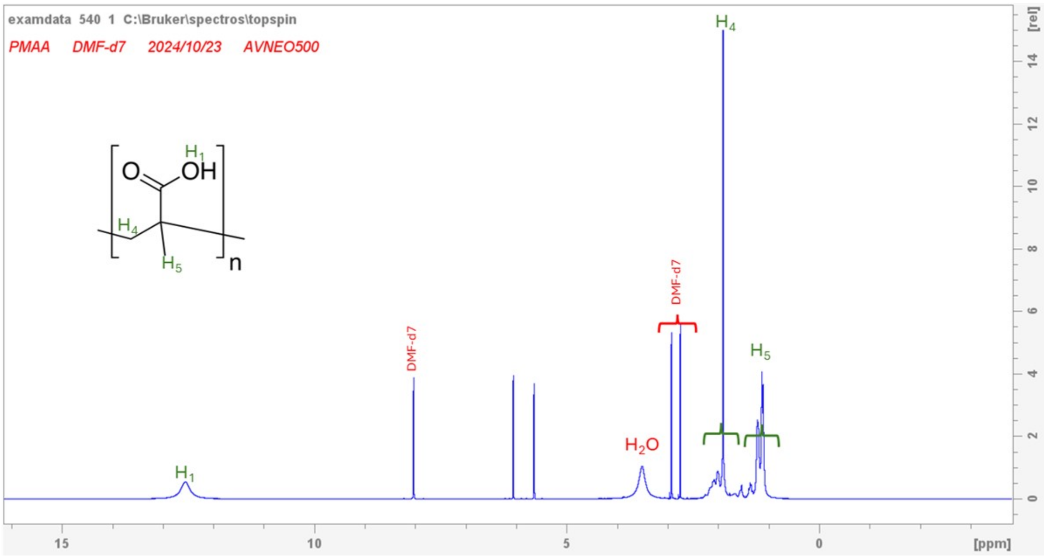
examdata 540 1 C:\Bruker\spectros\topspin
PMAA DMF-d7 2024/10/23 AVNEO500
H1
OH
O
H4
H5
n
DMF-d7
DMF-d7
H2O
H4
H5
H1
15
10
5
0
[ppm]
[rel]
14
12
10
8
6
4
2
0

(d)

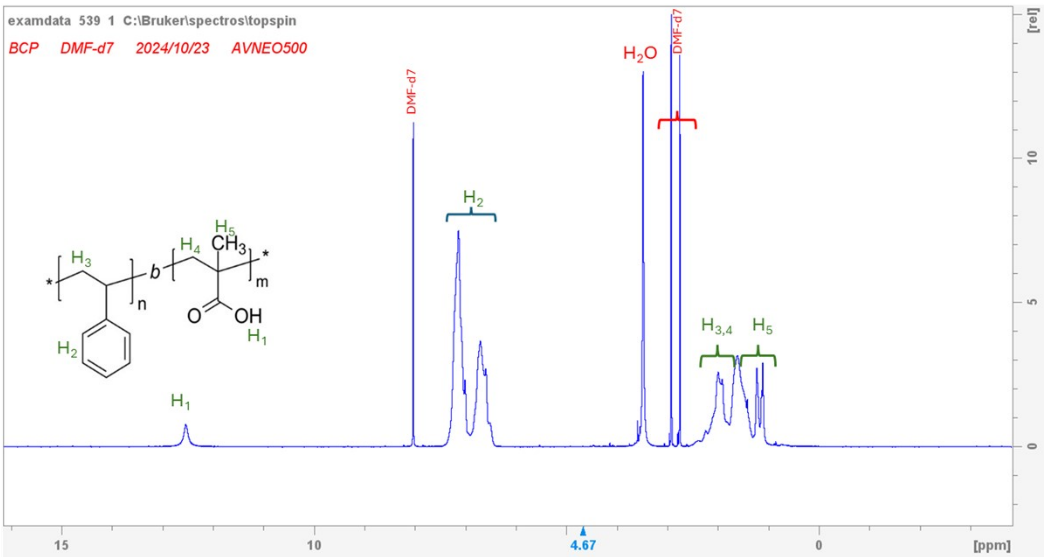
examdata 539 1 C:\Bruker\spectros\topspin
BCP DMF-d7 2024/10/23 AVNEO500
H3
H4
H5
CH3
n
b
m
O
OH
H1
H2
DMF-d7
H2
H2O
DMF-d7
H3,4
H5
H1
15
10
4.67
0
[ppm]
[rel]
10
5
0

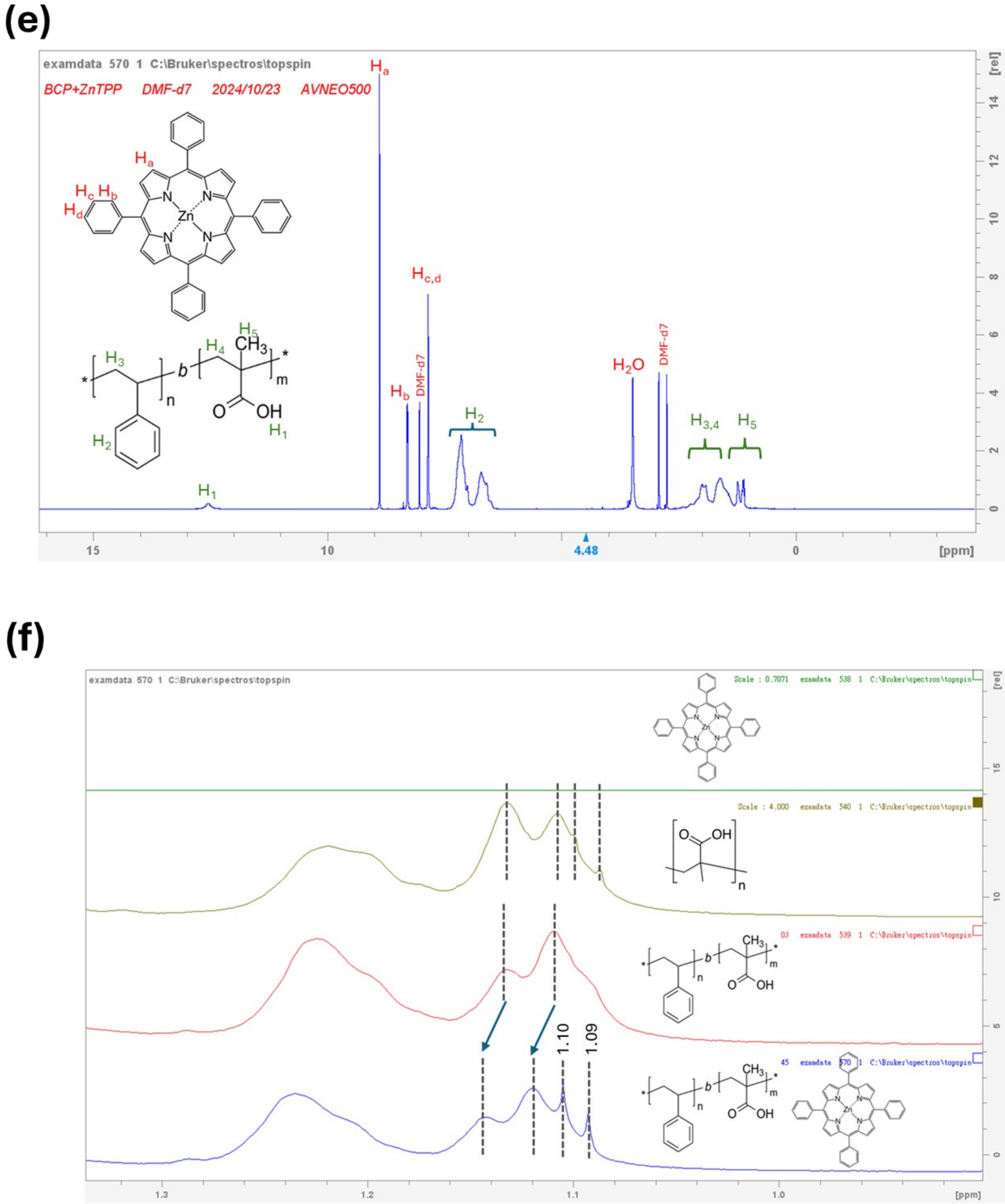

Figure S2. Solution ^{1}H NMR spectra of (a) ZnTPP, PMAA, PS-*b*-PMAA and PS-*b*-PMAA/ZnTPP, (b)ZnTPP, (c) PMAA, (d) PS-*b*-PMAA and (e) PS-*b*-PMAA/ZnTPP. (f) ZnTPP, PMAA, PS-*b*-PMAA and PS-*b*-PMAA/ZnTPP with the spectra ranged from 1.35 ppm to 0.99 ppm.

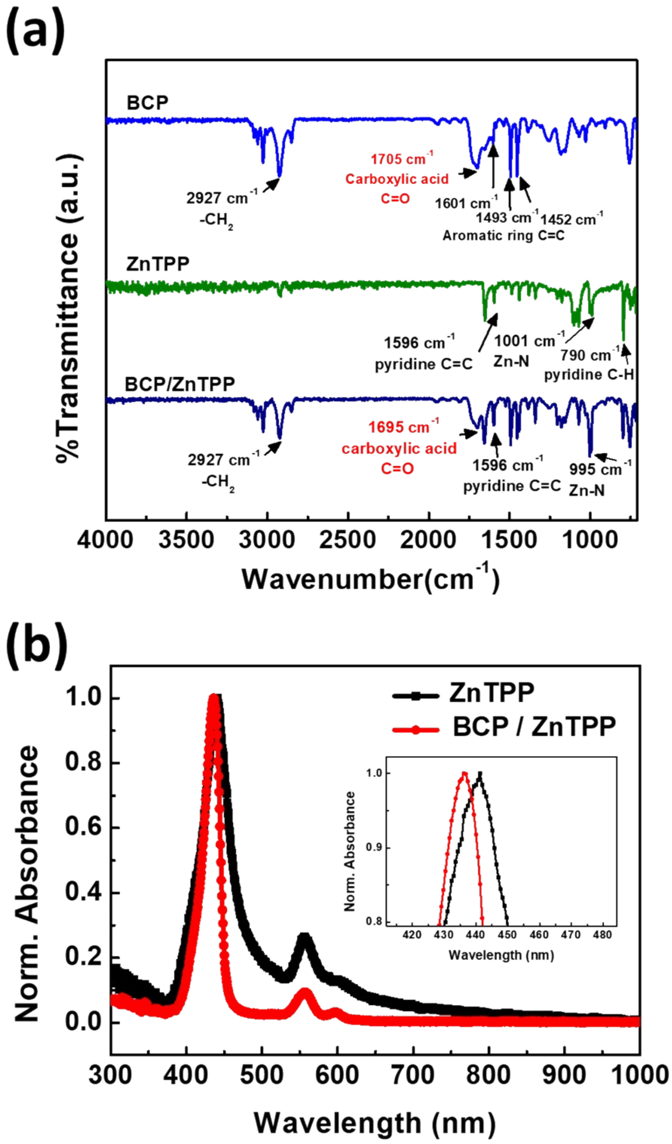

Figure S3. (a)FTIR spectra of BCP, ZnTPP and BCP/ZnTPP film to confirm the chelating effect between BCP and ZnTPP. (b) The absorption spectra of ZnTPP and BCP/ZnTPP film.

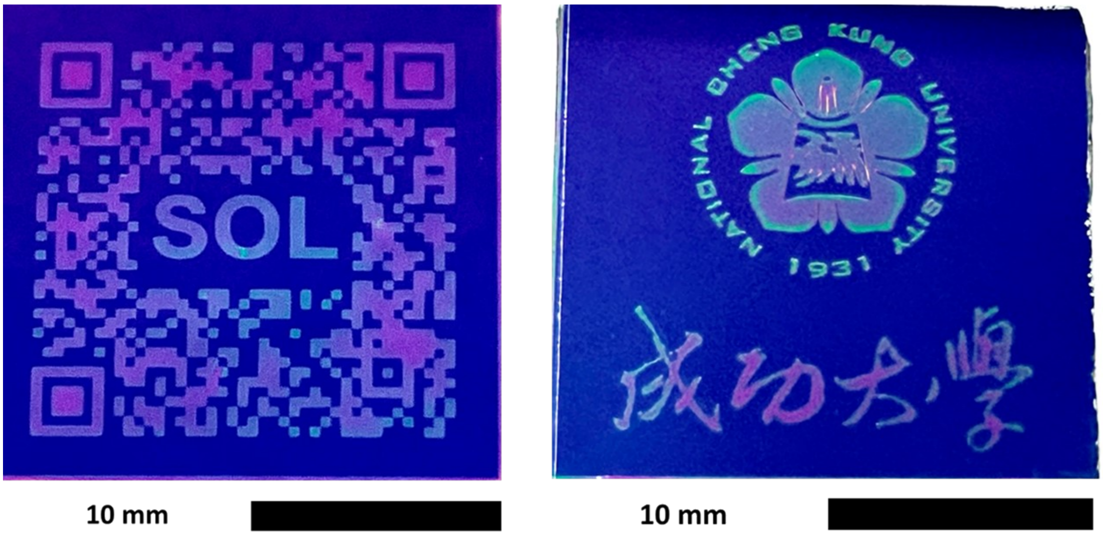

Figure S4. Photo-patterned DPP-DTT film with millimeter-scale dimension.

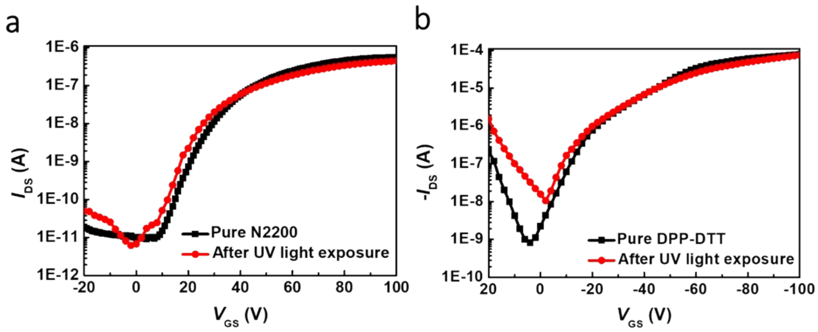

Figure S5. Stability test of conjugated polymer under UV light exposure. Transfer curves of (a)pure N2200 derived FET and (b) pure DPP-DTT derived FET.

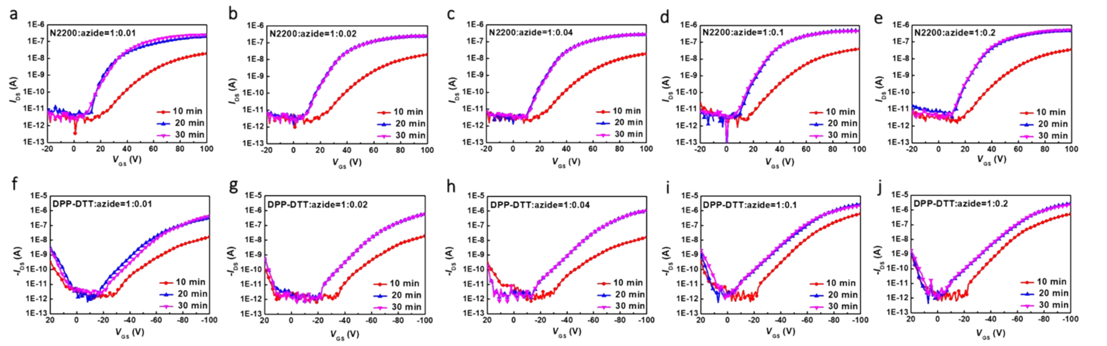

Figure S6. Transfer curves of photo-patterned *n*-type OFETs with N2200 to azide ratio ranged from (a)1:0.01, (b)1:0.02, (c)1:0.04, (d)1:0.1 to (e)1:0.2. Transfer curves of photo-patterned *p*-type OFET with DPP-DTT to azide ratio ranged from (f)1:0.01, (g)1:0.02, (h)1:0.04, (i)1:0.1 to (j)1:0.2. The transfer characteristics of the *n*-type OFETs were recorded by sweeping the gate voltage (V_{GS}) between -20 and 100 V under a fixed drain voltage (V_{DS}) of 100 while the transfer characteristics of the *p*-type OFETs were recorded by sweeping the gate voltage (V_{GS}) between 20 and -100 V under a fixed drain voltage (V_{DS}) of -100 V.

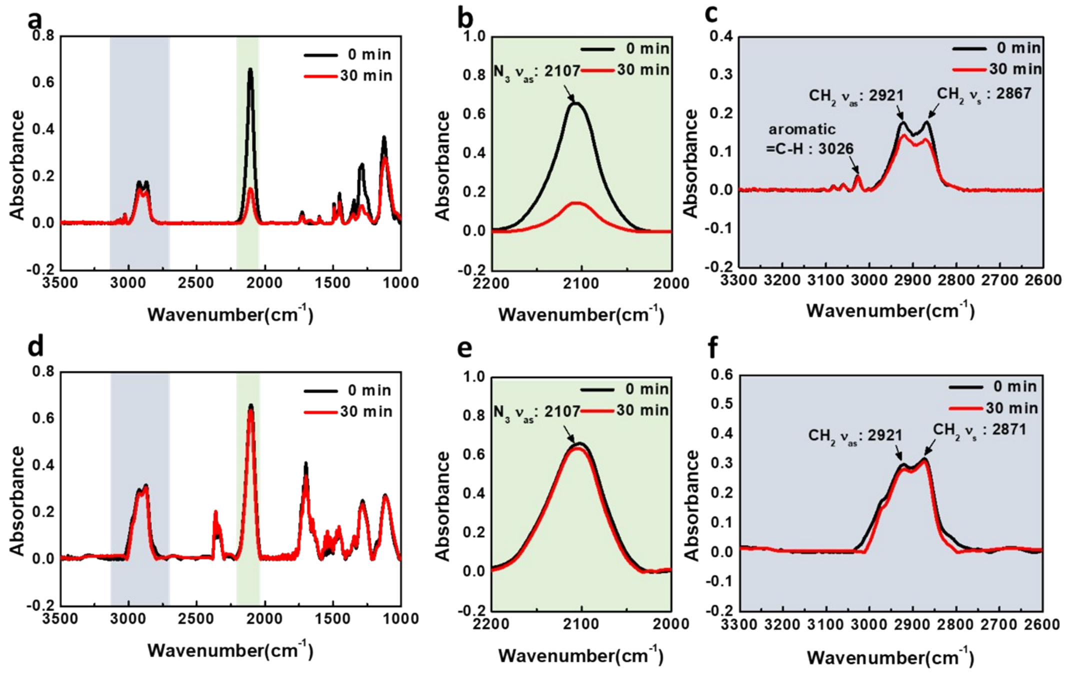

Figure S7 FTIR spectra of homopolymer and azide blend films before and after UV light exposure: (a) PS and azide blend film with enlarged region ranged from (b) 2200 cm^{-1} to 2000 cm^{-1} and (c) 3300 cm^{-1} to 2600 cm^{-1}; (d) PMAA and azide blend film with enlarged region ranged from (e) 2200 cm^{-1} to 2000 cm^{-1} and (f) 3300 cm^{-1} to 2600 cm^{-1}.

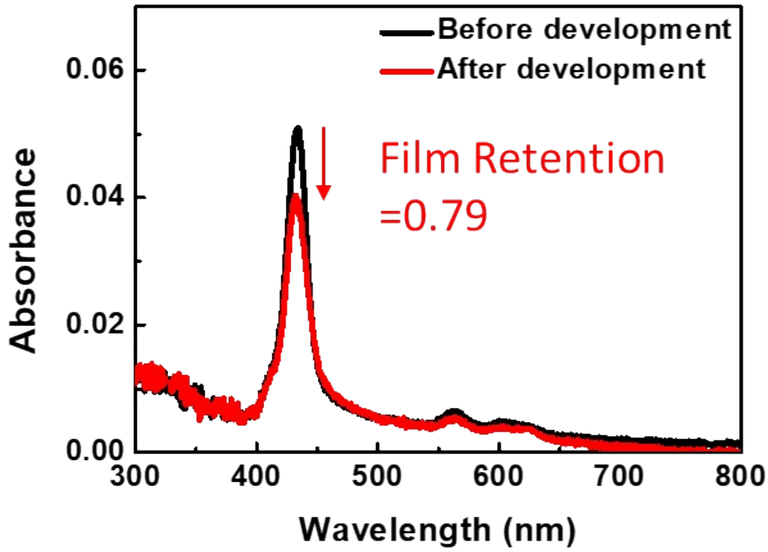

Figure S8. Absorption spectra of photo-crosslinked BCP/ZnTPP before and after development.

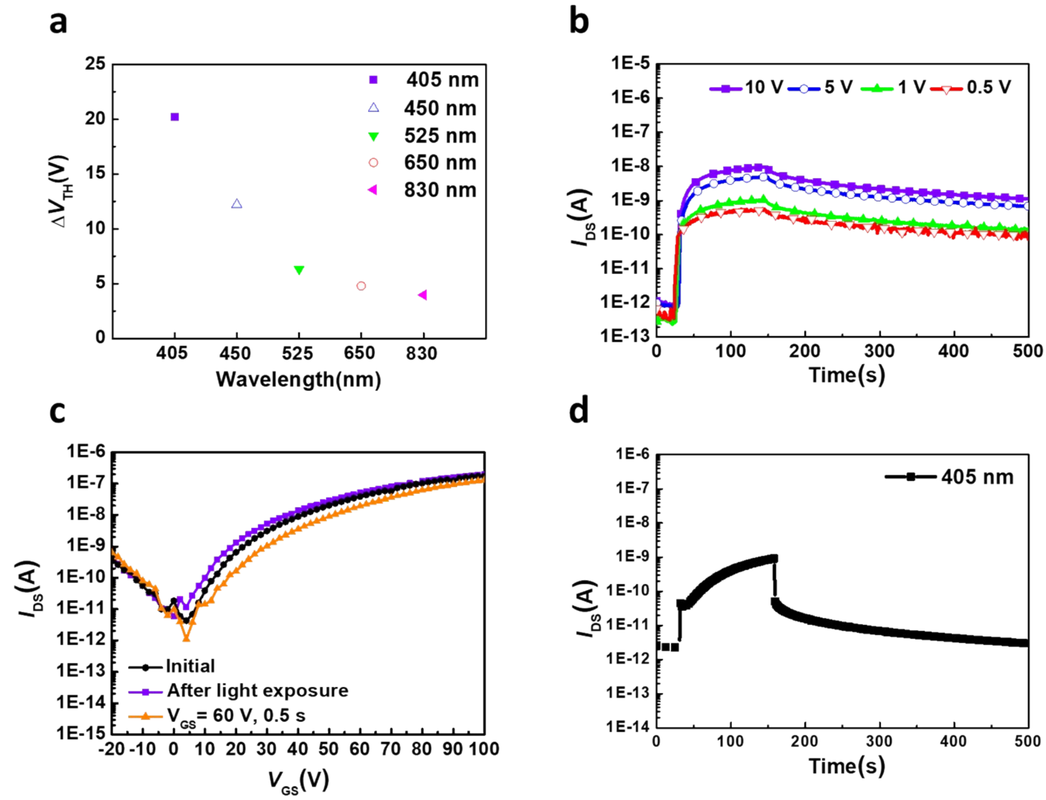

Figure S9. (a) The memory window of BCP/ZnTPP/N2200 based photomemory under different light sources. (b) The temporal I_{DS} under different V_{DS} ranged from 0.5 V to 10 V (405 nm, 60 mWcm^{-2}). (c) Transfer characteristics at V_{DS}=100 V of the BCP/N2200 OFET at initial state, under 405 nm light illumination (60 mWcm^{-2}) for 120 s and erasing at V_{GS}=60 s for 0.5 s. (d) The photo-responsive current toward time for the BCP/N2200 OFET under 405 nm illumination (120 s, 60 mW cm^{-2}) at V_{DS} =100 V.

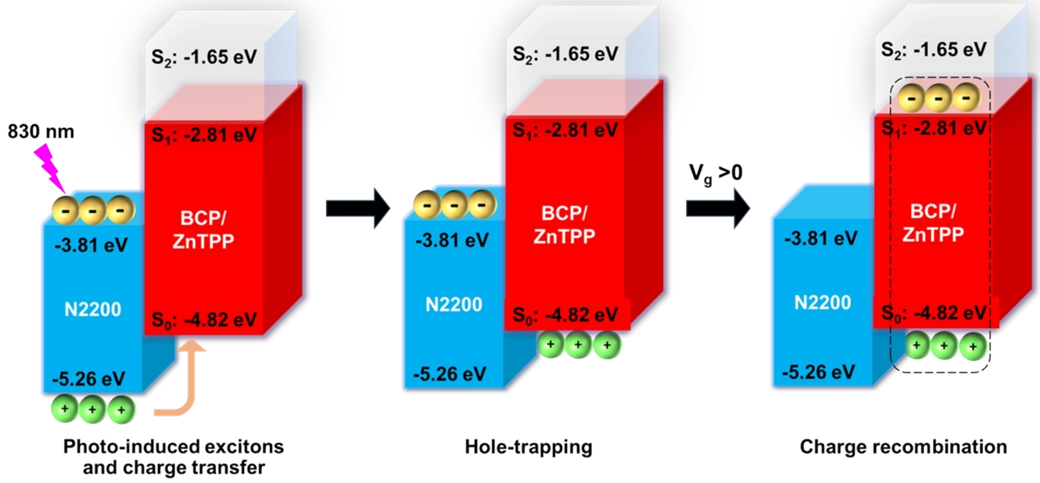

Figure S10. The proposed mechanism of photo-recordable behavior by lower photon energy.

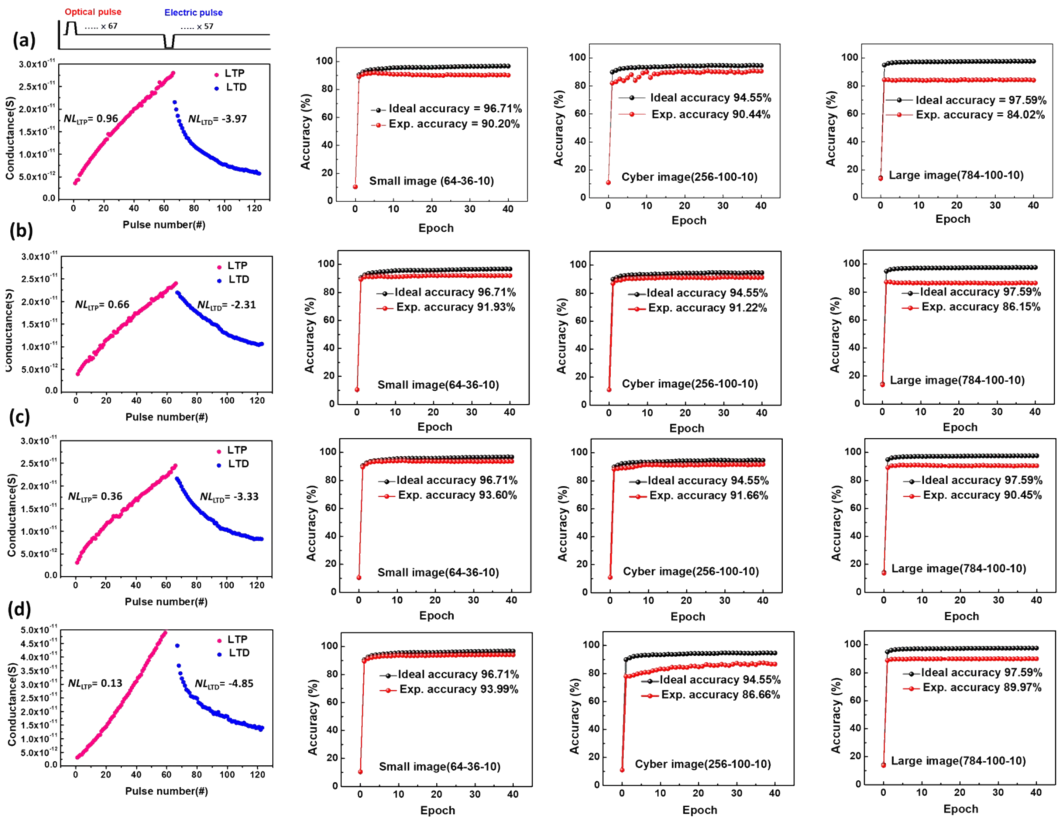

Figure S11. Four cycles of repeated LTP and LTD response by optical and electric pulse trains and the corresponding accuracy. (a) first cycle, (b)second cycle, (c) third cycle and (d) fourth cycle.

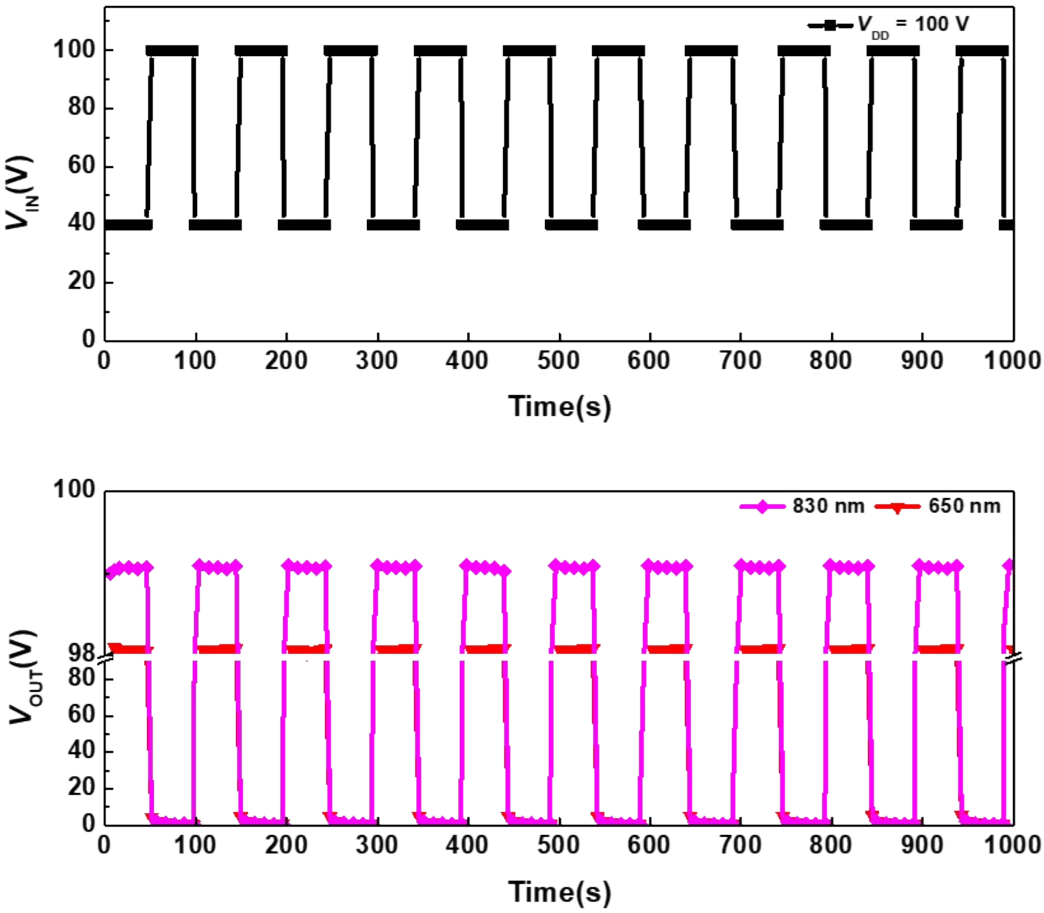

Figure S12. Switching characteristics of the photo-programmable inverter under 830 nm and 650 nm light stimuli.

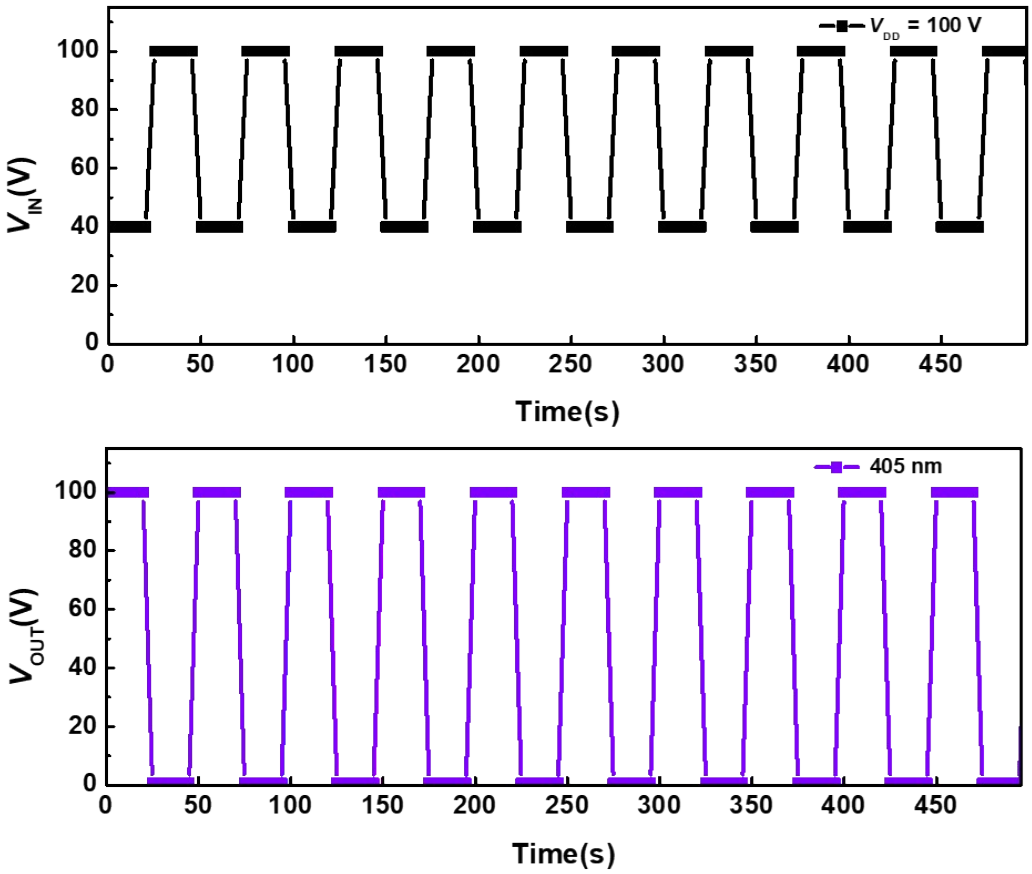

Figure S13. Time traces of the input and output voltage for inverter consisting of DPP-DTT based OFET and BCP/N2200 based OFET under 405 nm light illumination.